Biochemistry and Biophysics Reports 33 (2023) 101435

Contents lists available at ScienceDirect

Biochemistry and Biophysics Reports

journal homepage: www.elsevier.com/locate/bbrep

The pH-responsive precipitation–redissolution of the CspB fusion protein, CspB50TEV-Teriparatide, triggered by changes in secondary structure

Hayato Nagano [a,b,*], Teruhisa Mannen [a], Yoshimi Kikuchi [a], Kentaro Shiraki [b]

[a] Research Institute for Bioscience Product & Fine Chemicals, Ajinomoto Co., Inc., 1-1 Suzuki-cho, Kawasaki, 2108681, Japan
[b] Faculty of Pure and Applied Sciences, University of Tsukuba, 1-1-1 Tennodai, Tsukuba, Ibaraki, 305-8573, Japan

ARTICLE INFO

Keywords:
Cell surface protein B
pH-responsive and reversible precipitation-redissolution
Protein secondary structure
Protein inter-molecular interaction
Protein purification
Corynebacterium glutamicum

ABSTRACT

Cell surface protein B (CspB) fusion proteins can undergo reversible pH-responsive precipitation–redissolution. A pH-responsive precipitation–redissolution of CspB tag purification (pPRCP) method was established for protein purification using this property. However, the mechanism of the pH-responsive precipitation of CspB fusion proteins is unknown, which has made it difficult to set process parameters for pPRCP. In this study, we investigated the mechanism of the pH-responsive precipitation of CspB fusion proteins using CspB50TEV-Teriparatide (CspB-teri) as a model. As expected, CspB-Teri was reversibly precipitated at acidic pH. By contrast, CspB-Teri was not precipitated under unfolding conditions induced by trifluoroethanol, urea, or guanidine hydrochloride, even at acidic pH. The conformation of CspB-Teri changed to a β-sheet-rich structure as the pH decreased, followed by the formation of intermolecular interactions, which caused precipitation. The particle size of the CspB-Teri precipitate increased in a protein concentration-dependent manner. These results indicated that the pH-responsive precipitation of CspB-Teri is triggered by the formation of a β-sheet structure in response to decreasing pH, and the growth of the precipitate particles occurred through intermolecular interactions.

1. Introduction

Cell surface protein B (CspB) is a major extracellular secretion protein of *Corynebacterium glutamicum* [1]. CspB forms a self-assembled hexagonal 2D lattice structure and forms the S-layer comprising the cell wall in *C. glutamicum* [2–5]. CspB fusion proteins (CspB-tagged proteins), in which the *N*-terminal fragment of CspB is genetically fused to a target protein, can be reversibly precipitated in response to changes in pH [6]. The CspB fusion protein is soluble at neutral pH and is precipitated at acidic pH; the precipitate can then be fully redissolved at neutral pH. A purification method using a CspB tag, named "pH-responsive precipitation and redissolution of CspB tag purification" (pPRCP), has been reported using CspB50TEV-Teriparatide (CspB-Teri). CspB-Teri is composed of three regions, a 50 amino acid sequence from the *N*-terminus of CspB, a tobacco etch virus (TEV) protease recognition site, and teriparatide, which is a biopharmaceutical peptide used for the treatment of osteoporosis [7,8]. Briefly, CspB-Teri is precipitated at acidic pH, followed by the removal of impurities in the solution by centrifugation. The precipitated CspB-Teri is redissolved at neutral pH by addition of alkaline solution, and the purified CspB-Teri is obtained in the soluble state. The pH-responsive precipitation–redissolution of CspB fusion proteins is also affected by the solution conditions. In the presence of arginine, the solubility of the impurities increases, which can improve the purification yield of CspB fusion proteins [9]. Furthermore, kosmotropic ions can shift the pH value at which the CspB fusion protein is precipitated to neutral or basic conditions [10]. Investigation of the ability to control the solution state of CspB fusion proteins with additives will help determine the optimal solution conditions for purification of the proteins.

The precipitation and aggregation of proteins result from complex interactions, such as hydrophobic interactions between protein molecules [11], electrostatic interactions [12,13], and π–π interactions in the aromatic rings of aromatic amino acids [14]. The aggregation of proteins often changes their secondary structure, for example in amyloid formation [15,16]. Circular dichroism (CD) and Fourier transform infrared (FTIR) spectrometry are effective tools for the analysis of protein secondary structures to examine the mechanisms of protein aggregation and the change of protein activity [17–22]. For example, the secondary structure of amyloid-$\beta_{1\text{-}42}$ changes from a soluble monomer with a random coil form to an insoluble aggregate with a β-sheet structure, which can be monitored by the CD spectra [23]. Attenuated total reflectance FTIR spectrometry (ATR-FTIR) can be used to compare the solution state of the native protein form and the precipitated state of the

* Corresponding author. Faculty of Pure and Applied Sciences, University of Tsukuba, 1-1-1 Tennodai, Tsukuba, Ibaraki, 305-8573, Japan.
E-mail address: hayato.nagano01.dh2@asv.ajinomoto.com (H. Nagano).

https://doi.org/10.1016/j.bbrep.2023.101435
Received 8 December 2022; Received in revised form 17 January 2023; Accepted 25 January 2023

Abbreviations

C. gultamicum	Corynebacterium glutamicum
CORYNEX	Corynebacterium glutamicum protein expression system
CspB	cell surface protein B
CspB-Teri	CspB50TEV-Teriparatide;
pPRCP	pH-responsive precipitation-redissolution of CspB tag purification
CFB	cell-free broth
RP-HPLC	reverse phase high-performance liquid chromatography
TEV	tobacco etch virus
CD	circular dichroism
SDS-PAGE	sodium dodecyl sulfate-polyacrylamide gel electrophoresis
ATR-FTIR	attenuated total reflectance Fourier transform infrared spectrometry
TFE	trifluoroethanol
Gdn-HCl	guanidine hydrochloride.

aggregated protein form [24,25]. It is generally believed that content of β-sheet structure is increased in aggregates, stress-induced insoluble proteins, and heat-induced gelled proteins, compared with the native form of the protein [26,27].

In this study, we investigated the mechanism for the pH-responsive precipitation of CspB fusion proteins using solution additives. It has previously been shown that the concentration of the CspB fusion protein did not have an appreciable effect on the precipitation pH [10]. Thus, we hypothesized that intermolecular interactions are not a major driving force for pH-responsive precipitation. Herein, we investigated the pH-responsive precipitation of CspB-Teri in the presence of the protein denaturants urea, guanidine hydrochloride (Gdn-HCl), and trifluoroethanol (TFE). The secondary structure of the CspB-Teri determined by CD and ATR-FTIR showed that the secondary structure of the protein underwent a reversible change that correlated with the change between the precipitation and dissolution states. We concluded that a change in the secondary structure was responsible for the reversible pH-responsive precipitation–redissolution behavior of CspB-Teri.

2. Materials and methods

2.1. Materials

TFE and NaOH were from Fujifilm Wako Pure Chemical Corp., Osaka, Japan. Gdn-HCl, Tris (hydroxymethyl)-1,3-propanediol), HCl, acetonitrile (HPLC grade), and ammonium acetate were from Nacalai Tesque Inc., Kyoto, Japan. NaCl was from Junsei Chemical Co., Ltd., Tokyo, Japan. Urea was from Merck KGAA, Darmstadt, Germany.

2.2. Methods

2.2.1. Bacterial strain and design of the fusion protein

A CspB fusion protein, CspB-Teri, was constructed, which comprised a CspB fragment, the TEV protease cleavage recognition site, and teriparatide. The amino acid sequence of CspB-Teri is shown in our previous reports [6,7,10]. The amino acid sequence of CspB50 and TEV recognition sequence (underlined) and Teriparatide (bold) were shown below.

CspB50TEV-**Teriparatide**

QETNPTFNINNGFNDADG-
STIQPVEPVNHTEETLRDLTDSTGAY-
LEEFQYENLYFQ**SVSEIQLMHNLGKHLNSMERVEWLRKKLQDVHNF**

CspB-Teri composes of 90 amino acid residues with the isoelectric point of pH 4.3. CspB-Teri was prepared using the *C. glutamicum* secretion protein expression system CORYNEX® as described previously [28], which was provided by Ajinomoto Co., Inc.

2.3. Expression, fermentation, and purification of CspB-Teri

The expression and fermentation of CspB-Teri was performed as previously reported [7,10]. The culture supernatant that expressed CspB-Teri was purified by pPRCP according to our previous reports [7,10]. The CspB-Teri purified by pPRCP was further purified using Source 15RPC (Cytiva, Marlborough, MA, USA) packed to FineLINE™ Pilot35 (Cytiva, Marlborough, MA, USA). The Source 15RPC chromatography was performed using buffer A (20 mM ammonium acetate, 10% acetonitrile) and buffer B (20 mM ammonium acetate, 80% acetonitrile) with a gradient elution of 0%–50% buffer B for 20 column volumes at 150 cm/h. The material purified by Source 15RPC was exchanged into 20 mM Tris-HCl, pH 8.0 for the spectroscopic measurements.

2.4. Calculation of the precipitation ratio of CspB-Teri

Evaluation of the precipitation ratio was performed as previously reported and is shown below [10]. CspB-Teri in the evaluation sample was quantified by reverse phase high-performance liquid chromatography (RP-HPLC) as previously described [10] to measure the concentration of CspB-Teri.

$$\text{Precipitation ratio } [\%] = 100 - (A_{conc.} / B_{conc.} \times \quad 100)$$

$A_{conc.}$: Measured concentration of CspB-Teri in the evaluation sample.

$B_{conc.}$: Expected concentration of CspB-Teri without precipitation in the evaluation sample considering the volume of the added acid solution and the sampling volume.

CD.

The far-ultraviolet (UV) CD spectra were measured for 0.3 mg/mL CspB-Teri in 20 mM Tris-HCl buffer, with and without additives. The far-UV CD spectra were measured at 25 °C using a J-820 spectropolarimeter (Jasco Co., Tokyo, Japan) with an ASU-800 auto sampler (Jasco Co., Tokyo, Japan) in the range of 250 to 200 nm at a scanning rate of 100 nm/min. Each sample was loaded in a quartz cell with a 1-mm path length.

2.5. Sodium dodecyl sulfate-polyacrylamide gel electrophoresis (SDS-PAGE)

SDS-PAGE was performed using 12% NuPAGE® Bis-Tris, 1 mm, mini protein gel (Thermo Fisher Scientific, Waltham, MA, USA) with NuPAGE® SDS 2-(*N*-morpholino) ethane sulfonic acid (MES) running buffer and NuPAGE® Antioxidant according to the manufacturer's instructions. The protein bands were stained using Quick-CBB Coomassie stain (Fujifilm Wako Pure Chemical Corporation, Osaka, Japan) and the gel images were processed using Image Quant TL (Cytiva, Marlborough, MA, USA).

2.6. ATR-FTIR

ATR-FTIR spectra were recorded using a FT/IR4600 (Jasco Co., Tokyo, Japan) with ATR accessory, ATR PRO Penta (Jasco Co., Tokyo, Japan), and a mercury, cadmium, and tellurium detector. To obtain the spectra, 10 μL of 20 mg/mL samples were applied on a Ge prism. The spectra of the blank buffer (20 mM Tris-HCl that was adjusted to the sample pH) was subtracted from the sample spectra. Data analysis and processing, including second derivative analysis, were performed using the Spectra manager software (Jasco). To obtain the final FTIR absorbance spectra, blank buffer (no protein) spectra was subtracted from the

actual protein sample spectra. To compare the samples, the baseline of the FTIR spectra were corrected to reveal the amide I band region, 1600–1700 cm^{-1}. FTIR spectra were normalized to the same band intensity of the amide I band at 1654 cm^{-1} in this experiment.

2.7. Optical microscope

Non-filtered CspB-Teri in 20 mM Tris-HCl was observed at pH 8.0; pH 4.0, adjusted by adding HCl; and pH 7.0, adjusted by adding NaOH. An aliquot of each sample (10 μL) was transferred to a microscopy slide equipped with a microscope cover glass. Samples were observed using an optical microscope BZ-X800 (Keyence) with a 10 × eyepiece lens and 10, 20×, and 100 × objective glasses.

The amino acid sequences used for CspB and teriparatide were from GenBank (accession numbers **BAV24076.1** and **AAQ51502.1**, respectively) [6].

3. Results

3.1. CspB-Teri was not precipitated in TFE solution even at acidic pH

It has been previously reported that the precipitation of CspB-Teri did not depend on the protein concentration [10]. Thus, we hypothesized that the pH-responsive precipitation of CspB-Teri is triggered by a change in the secondary structure, followed by the precipitation of CspB-Teri caused by intermolecular interactions.

TFE converts the structure of proteins into an α-helical form in a concentration-dependent manner [29]. Therefore, the structure of CspB-Teri was altered using various concentrations of TFE solutions, and then the pH of the TFE-induced CspB-Teri solutions was decreased to cause precipitation. Fig. 1A shows the far-UV CD spectra of CspB-Teri in solutions with various concentrations of TFE. The CD spectra of CspB-Teri in the absence of TFE showed a α-helical structure. With increasing concentrations of TFE, negative maxima at 215 and 222 nm were observed, which are typical of an α-helical structure. This result indicated that, as expected, the conformation of CspB-Teri changed to an α-helical structure in a TFE concentration-dependent manner. Fig. 1B shows the precipitation ratio of CspB-Teri at pH 4.0 for various TFE concentrations. CspB-Teri was completely precipitated at concentrations below 20% TFE. With increasing concentrations of TFE, CspB-Teri was progressively solubilized between 20% and 40% TFE at pH 4.0. These results suggested a relationship between the pH-responsive precipitation and the secondary structure of CspB-Teri.

3.2. Denaturants suppressed the pH-responsive precipitation of CspB-Teri

Fig. 2 shows the pH-responsive precipitation of CspB-Teri in the presence of TFE and the protein denaturants urea and Gdn-HCl. As reported previously [10], CspB-Teri was precipitated at approximately pH 5.8 without any additives. Similarly, CspB-Teri was precipitated at approximately pH 6.5 in the presence of 0.5 M NaCl. In both cases, the protein was completely precipitated in acidic conditions. By contrast, CspB-Teri started to precipitate at pH 5.4 in 50% TFE, but only approximately 20% of the CspB-Teri was precipitated, even at pH 4.0. Similarly, CspB-Teri did not precipitate at acidic pH in the presence of 6 M urea or 5 M Gdn-HCl. High concentrations of urea or Gdn-HCl resulted in unfolding of the protein structure, and in a solution of 50% TFE, the structure was changed to a α-helical form; hence, it is likely that a specific structure is necessary for the pH-responsive precipitation of CspB-Teri at acidic pH.

Plots of the relationship between the pH value and precipitation ratio of CspB-Teri in 20 mM Tris-HCl with no additives (closed square), 0.5 M NaCl (closed circle), 5 M Gdn-HCl (closed triangle), 6 M urea (closed rhombus), and 50% TFE (cross mark).

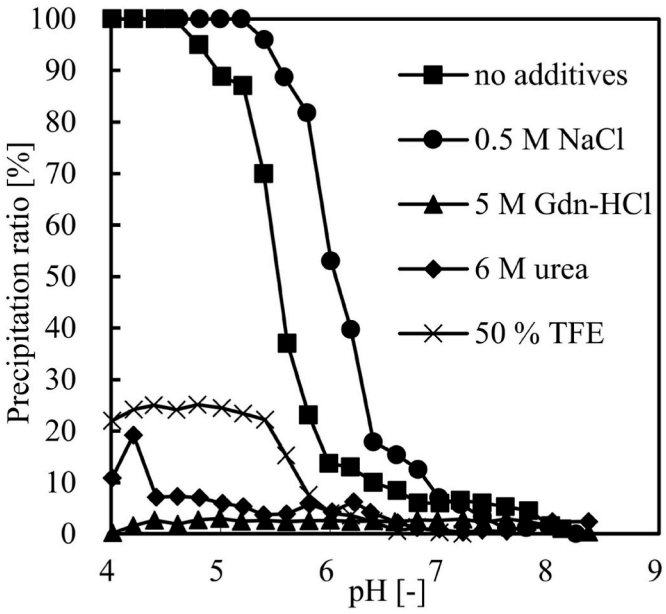

Fig. 2. pH-responsive precipitation of CspB-Teri under unfolding conditions.

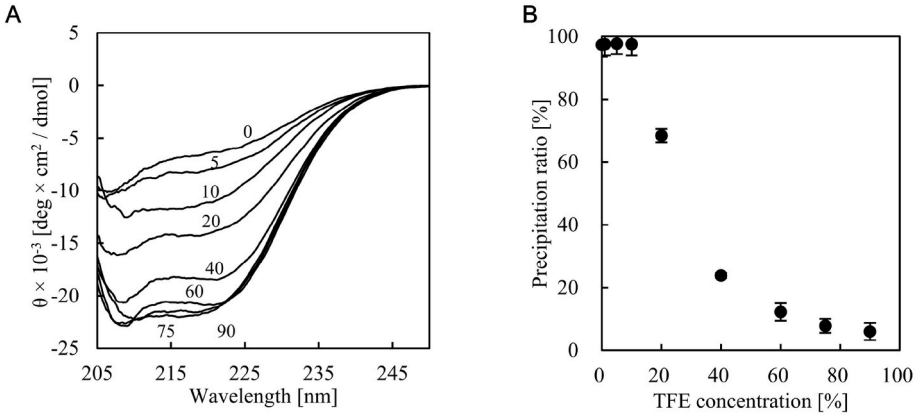

Fig. 1. pH-responsive precipitation of CspB-Teri in TFE solution.
(A) TFE-dependent structural transition of CspB-Teri at pH 8.0 with 0%–90% TFE measured by CD. The numbers refer to the TFE concentration as a percentage by volume. (B) The precipitation ratio of CspB-Teri at pH 4.0 for various concentrations of TFE.

3.3. Secondary structure of CspB-Teri under acidic conditions with additives

The secondary structure of the protein in the pH-responsive precipitation of CspB-Teri was investigated by far-UV CD (Fig. 3). The CD spectra of CspB-Teri in 20 mM Tris-HCl, pH 8.5 without any additives showed as the initial secondary structure before the structure changes by pH and additives in dash line. The CD spectra of CspB-Teri without additives (Fig. 3A) showed a gradual decrease of an ellipticity at 218 nm with decreasing pH values. Note that CspB-Teri started to precipitate during the monitored pH values. Similarly, the CD spectra of CspB-Teri with 0.5 M NaCl (Fig. 3B) showed a gradual decrease of an ellipticity at 218 nm with decreasing pH values. The shapes of the CD spectra of CspB-Teri with and without NaCl indicated that the structure contained β-sheet content at the pH values where precipitation occurred. The CD spectra of CspB-Teri in 50% TFE showed typical α-helical structure at all pH values but slightly decrease of an ellipticity at 218 nm with decreasing pH (Fig. 3C). This result indicated that a part of the secondary structure in the 50% TFE solution changed and CspB-Teri precipitated. This data was accordance with the data that the precipitation ratio of CspB-Teri was around 20% in 50% TFE condition shown in Fig. 1B. This result suggested that most of the secondary structure of CspB-Teri in TFE condition was α-helical structure but partially formed the initial structure. In contrast, in the presence of 5 M Gdn-HCl (Fig. 3D) or 6 M urea (Fig. 3E), CspB-Teri was fully unfolded even at acidic pH values. These data indicated that the secondary structure plays an important role in the pH-responsive precipitation of CspB-Teri.

The pH-dependent secondary structure transition of CspB-Teri measured by CD during pH-responsive precipitation in the presence of (A) no additive, (B) 0.5 M NaCl, (C) 50% TFE, (D) 5 M Gdn-HCl, and (E) 6 M urea. The dashed lines in each figure show the initial structure of CspB-Teri in 20 mM Tris -HCl at pH 8.5 without any additives.

3.4. CspB-Teri formed a β-sheet-rich secondary structure at precipitation

Fig. 4A shows the SDS-PAGE analysis of CspB-Teri. Briefly, a solution of CspB-Teri in 20 mM Tris-HCl (pH 8.0) was prepared, then, HCl was titrated into the CspB-Teri solution. Samples of the solution at pH 6.0, 5.6, and 4.0 were collected. Then, NaOH was added to the solutions to adjust the pH to 7.4 to redissolve the pH-responsive precipitate. The sample T which is not filtered shows the total amount of CspB-Teri in sample both precipitation and soluble state. The sample S shows the amount of soluble state of CspB-Teri which the precipitated CspB-Teri is removed by filtration. The sample P shows the amount of precipitation state of CspB-Teri which the soluble CspB-Teri is removed as supernatant by centrifuge and dissolved the precipitated CspB-Teri with 20 mM Tris-HCl, pH 8.5. As shown in Fig. 4A, CspB-Teri started to precipitate at pH 6.0 and was fully dissolved at pH 7.4.

Fig. 4B and C shows the results of ATR-FTIR spectroscopy for the soluble state before precipitation (pH 8.0), during the process of pH-responsive precipitation (pH 5.6 and 5.4), the precipitated state (pH 4.0), and the redissolved state after precipitation (pH 7.4). FTIR spectra were normalized to the peak at 1654 cm^{-1} in the amide I band (Fig. 4B). The peaks at 1624 and 1619 cm^{-1} increased with decreasing pH from pH 6.0 to 5.6 where precipitation occurred. The peak at 1624 cm^{-1} was prominent at pH 4.0 where the protein was completely precipitated. The spectra of the redissolved sample of CspB-Teri at pH 7.4 was completely overlapped with that at pH 8.0. These results indicated that the pH-responsive precipitation of CspB-Teri was related to the reversible secondary structure change observed by FTIR at 1624 and 1619 cm^{-1}. Note that the peaks in the FTIR spectra at approximately 1624 and 1620 cm^{-1} indicate an intermolecular β-sheet structure [26,30–33]. Thus, the

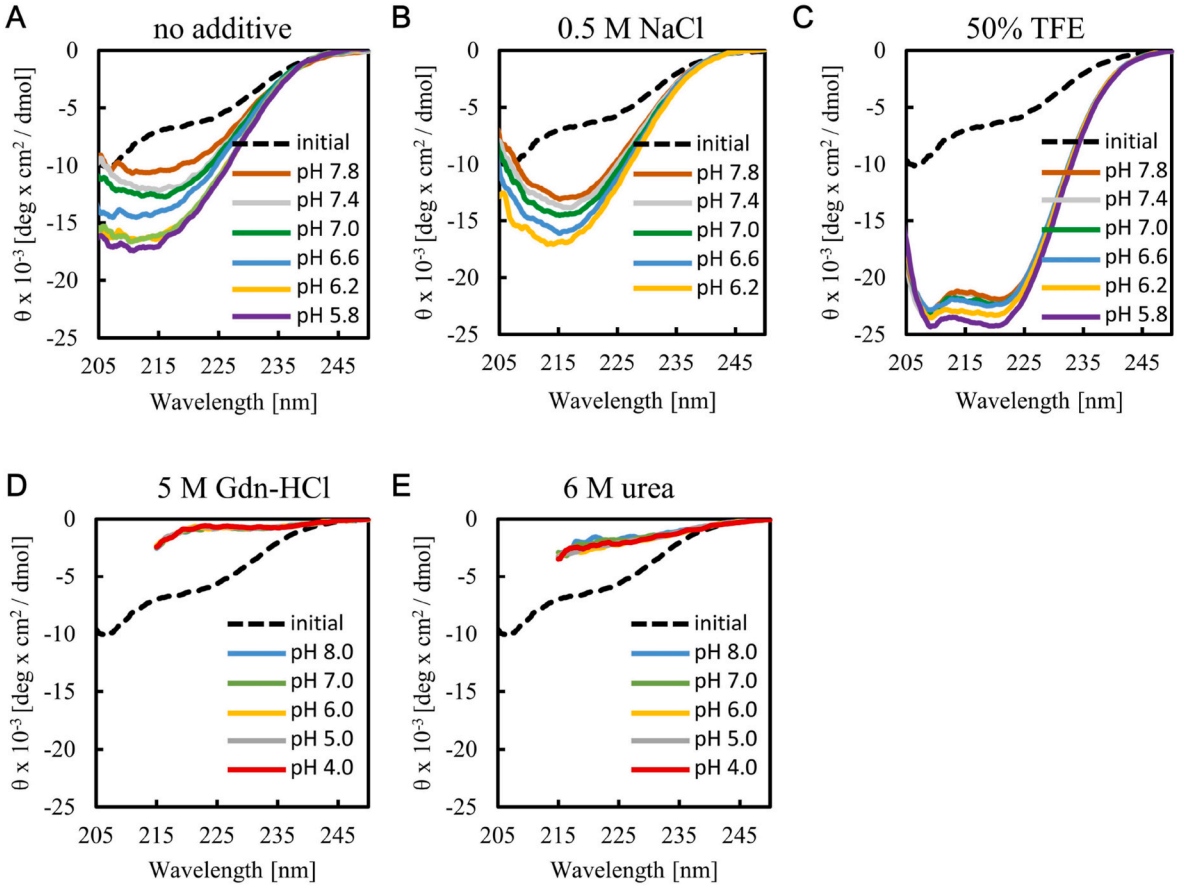

Fig. 3. The secondary structure transition of CspB-Teri during pH-responsive precipitation with various additives.

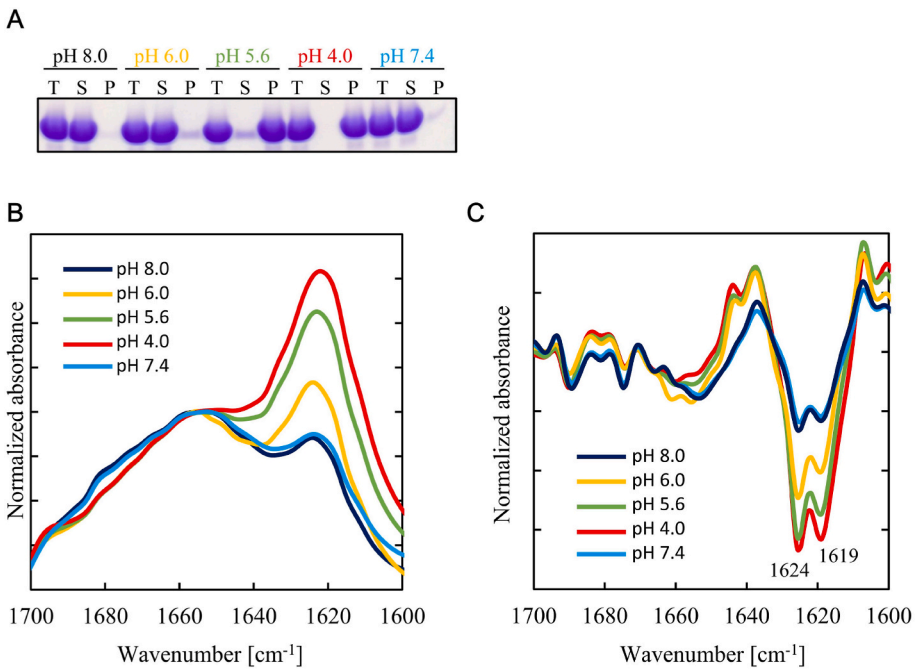

Fig. 4. Secondary structure transition between the solution state and precipitation state determined by ATR-FTIR spectrometry.
(A) SDS-PAGE analysis of CspB-Teri at various pH values. The data at pH 8.0, 6.0, 5.6, and 4.0 show the samples at the respective pH values, while the data at pH 7.4 is for the redissolved protein after precipitation. The sample T shows the total amount of CspB-Teri in sample both precipitation and soluble state. The sample S shows the amount of soluble state of CspB-Teri which the precipitated CspB-Teri is removed by filtration. The sample P shows the amount of precipitation state of CspB-Teri which the soluble CspB-Teri is removed by centrifuge and dissolved the precipitated CspB-Teri with 20 mM Tris-HCl, pH 8.5.

conformation of CspB-Teri was changed to a β-sheet-rich structure as the pH decreased, followed by the formation of intermolecular interactions and precipitation.

3.5. The particle size of the precipitate of CspB-Teri increased with increasing protein concentrations

Fig. 5 shows the results of optical microscope observations of the

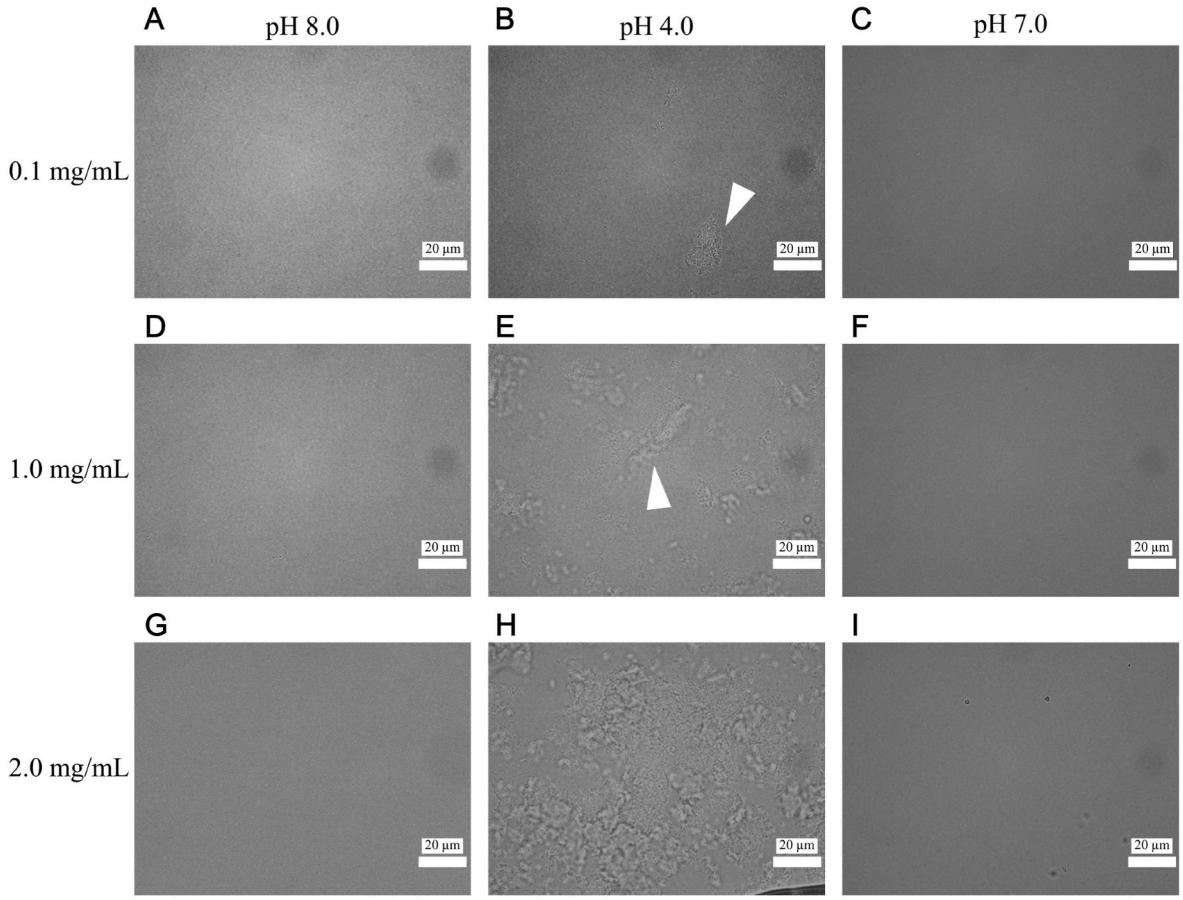

Fig. 5. Optical microscope images of soluble and precipitated states of CspB-Teri at different concentrations.

dissolved (pH 8.0), precipitated (pH 4.0), and redissolved (pH 7.0) states of CspB-Teri at protein concentrations of 0.1, 1.0, and 2.0 mg/mL. As expected, no precipitate was observed for all protein concentrations at pH 8.0 (Fig. 5A, D, and 5G) and pH 7.0 (Fig. 5C, F, and 5I). A precipitate was only observed at pH 4.0 (Fig. 5B, E, and 5H shown by the white arrow) and the particle size of the precipitate increased in a concentration-dependent manner.

The soluble (A, D, and G), precipitation (B, E, and G), and redissolved (C, F, and I) states of CspB-Teri at 0.1 mg/mL (A, B, and C), 1 mg/mL (D, E, and F), and 2 mg/mL (G, H, and I). White bar shows 20 μm.

4. Discussion

In the present study, we demonstrated that changes in the secondary structure of CspB-Teri were responsible for the pH-responsive precipitation. The results are briefly summarized as follows. (i) CspB-Teri did not precipitate in the presence of a high concentration of TFE, urea, or Gdn-HCl, even at acidic pH. (ii) The content of intermolecular β-sheet structure in CspB-Teri was increased in the process of pH-responsive precipitation. (iii) The particle size of the precipitate of CspB-Teri increased depending on the concentration of the protein. From these results, we discard the hypothesis that intermolecular interactions are not a major driving force for pH-responsive precipitation because CspB-Teri, which secondary structure changed to β-sheet rich, is formed a precipitate by intermolecular interaction of β-sheet rich structure. Then, we proposed a mechanism for the pH-responsive precipitation of CspB-Teri, shown in Fig. 6. Step (1) CspB-Teri at neutral pH is soluble and has the native secondary structure conformation. Under neutral conditions, CspB-Teri is less likely to associate with other molecules due to the electrostatic repulsion. Step (2) Under acidic conditions, the secondary structure of CspB-Teri changes to β-sheet-rich structure. Step (3) The β-sheet-rich proteins interact with each other without electrostatic repulsion at around isoelectric pH and then form precipitates. Step (4) On returning to a neutral pH, the secondary structure of CspB-Teri is transformed to the native structure and CspB-Teri is completely redissolved.

The pH-responsive precipitation of CspB-Teri did not occur in the presence of TFE, urea, or Gdn-HCl at concentrations that induced protein unfolding. This result is because the secondary structure of CspB-Teri was changed by the additives, resulting in the suppression of the intermolecular interactions in the β-sheet structure. In the presence of TFE, CspB-Teri cannot change to a β-sheet-rich structure because the secondary structure of CspB-Teri is transformed and maintained in an α-helix-rich conformation by TFE. Therefore, it was not possible for CspB-Teri to move to step (2) in Fig. 6 and the pH-responsive precipitation did not occur in the presence of TFE. Similarly, in the presence of Gdn-HCl or urea, CspB-Teri was not able to move to step (2) in Fig. 6 because the secondary structure of CspB-Teri was denatured and transformed to a random coil structure as shown in Fig. 3D and E and cannot be transformed to a β-sheet-rich structure.

Regarding the change in secondary structure of CspB-Teri, the secondary structure of Teriparatide was an α-helical peptide in pH 6.1 solution analyzed by CD spectroscopy and NMR spectroscopy [34]. In addition, the α-helical structure of Teriparatide was observed at pH 4.0 at which the pH responsive precipitation occurred [7]. These results indicate that the α-helical secondary structure of Teriparatide maintain even in pH 4.0. In this paper, we newly revealed that the secondary structure of CspB-Teri changes to β-sheet rich structure at pH 4.0. These data suggest that change in secondary structure to β-sheet at pH 4.0 is attributed to the property of the CspB50TEV.

Another important finding of this study is that the signals in the ATR-FTIR spectra at approximately 1624 cm $^{-1}$ are related to the β-sheet secondary structure observed in the pH-responsive precipitation. The presence of an increasing content of β-sheet structure has been previously observed using ATR-FTIR spectroscopy in protein aggregates, including inclusion bodies [26], the thermal aggregation of bovine IgG [35], and amyloid fibrils from hen lysozyme [36]. These examples support our hypothesis that the transition of the secondary structure to a β-sheet structure triggered the pH-responsive precipitation of the CspB fusion protein. In pPRCP, the precipitation pH is not suitable as the process parameter for pPRCP because the precipitation pH depends on the type of solution [10]. The intensity of the band at 1624 cm^{-1} in the ATR-FTIR spectra can be an effective process parameter because this changes in secondary structure occurs independently of solution condition. This finding should improve pPRCP as a purification method.

In conclusion, the pH-responsive precipitation of CspB-Teri is induced by a secondary structure transition to a β-sheet-rich structure, followed by intermolecular interactions. The secondary structure transition to a β-sheet-rich structure can be observed by increases in the band at 1624 cm^{-1} in the ATR-FTIR spectra and this change in band intensity will be able to be used as a process parameter for pPRCP.

Autor statements

Hayato Nagano: Investigation and writing, Teruhisa Mannen: Conceptualization, Yoshimi Kikuchi: Supervision, Kentaro Shiraki: Conceptualization, writing and Supervision. All authors read and approved the manuscript. The authors declare that they have no conflicts of interest.

Declaration of competing interest

The authors declare that they have no conflicts of interest.

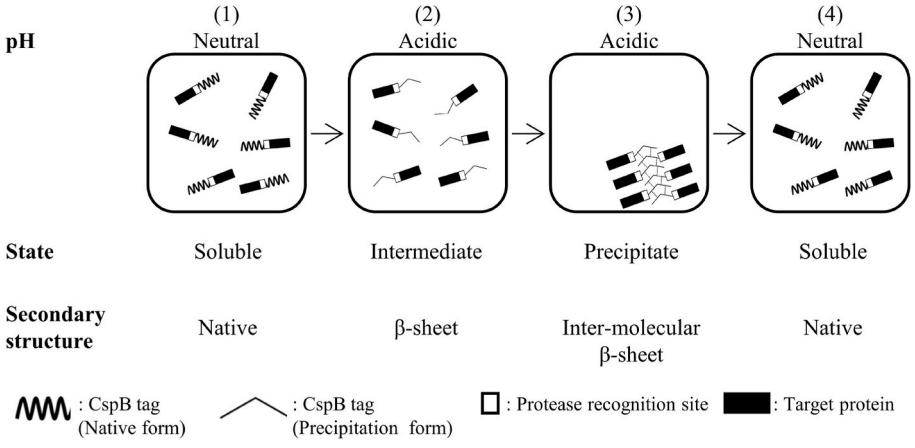

Fig. 6. Proposed mechanism for the pH-responsive precipitation of CspB-Teri.

Data availability

Data will be made available on request.

Acknowledgments

We are grateful for financial support from Ajinomoto Co., Inc. We also thank all members of the CORYNEX® research group of Ajinomoto Co., Inc and for helpful discussions.

References

[1] M. Chami, N. Bayan, J.-C. Dedieu, G. Leblon, E. Shechter, T. Gulik-Krzywicki, Organization of the outer layers of the cell envelope of Corynebacterium glutamicum: a combined freeze-etch electron microscopy and biochemical study, Biol. Cell. 83 (2–3) (1995) 219–229, https://doi.org/10.1016/0248-4900(96)81311-6.

[2] M. Chami, N. Bayan, J.L. Peyret, T. Gulik-Krzywicki, G. Leblon, E. Shechter, The S-layer protein of Corynebacterium glutamicum is anchored to the cell wall by its C-terminal hydrophobic domain, Mol. Microbiol. 23 (3) (1997) 483–492, https://doi.org/10.1046/j.1365-2958.1997.d01-1868.x.

[3] V. Puech, et al., Structure of the cell envelope of corynebacteria: importance of the non-covalently bound lipids in the formation of the cell wall permeability barrier and fracture plane, Microbiology 147 (5) (2001) 1365–1382, https://doi.org/10.1099/00221287-147-5-1365.

[4] S. Scheuring, H. Stahlberg, M. Chami, C. Houssin, J.-L. Rigaud, A. Engel, Charting and unzipping the surface layer of Corynebacterium glutamicum with the atomic force microscope, Mol. Microbiol. 44 (3) (2002) 675–684, https://doi.org/10.1046/j.1365-2958.2002.02864.x.

[5] N. Hansmeier, et al., Classification of hyper-variable Corynebacterium glutamicum surface-layer proteins by sequence analyses and atomic force microscopy, J. Biotechnol. 112 (1–2) (Aug. 2004) 177–193, https://doi.org/10.1016/j.jbiotec.2004.03.020.

[6] T. Nonaka, N. Tsurui, T. Mannen, Y. Kikuchi, K. Shiraki, A new pH-responsive peptide tag for protein purification, Protein Expr. Purif. 146 (Jun. 2018) 91–96, https://doi.org/10.1016/j.pep.2018.02.004.

[7] T. Nonaka, N. Tsurui, T. Mannen, Y. Kikuchi, K. Shiraki, Non-chromatographic purification of Teriparatide with a pH-responsive CspB tag, Protein Expr. Purif. 155 (Mar. 2019) 66–71, https://doi.org/10.1016/j.pep.2018.11.008.

[8] R. Lindsay, J.H. Krege, F. Marin, L. Jin, J.J. Stepan, Teriparatide for osteoporosis: importance of the full course, Osteoporos. Int. 27 (2016) 2395–2410, https://doi.org/10.1007/s00198-016-3534-6.

[9] S. Oki, T. Nonaka, K. Shiraki, Specific solubilization of impurities in culture media: arg solution improves purification of pH-responsive tag CspB50 with Teriparatide, Protein Expr. Purif. 146 (Jun. 2018) 85–90, https://doi.org/10.1016/j.pep.2018.02.001.

[10] H. Nagano, T. Mannen, Y. Kikuchi, K. Shiraki, Solution design to extend the pH range of the pH-responsive precipitation of a CspB fusion protein, Protein Expr. Purif. 195–196 (2022), 106091, https://doi.org/10.1016/j.pep.2022.106091. Aug.

[11] Y. Kuroda, Biophysical studies of protein solubility and amorphous aggregation by systematic mutational analysis and a helical polymerization model, Biophys Rev. 10 (2) (Jan. 2018) 473–480, https://doi.org/10.1007/s12551-017-0342-y.

[12] H. Wu, T.W. Randolph, Aggregation and particle formation during pumping of an antibody formulation are controlled by electrostatic interactions between pump surfaces and protein molecules, J. Pharmaceut. Sci. 109 (4) (2020) 1473–1482, Apr, https://doi.org/10.1016/j.xphs.2020.01.023.

[13] G.V. Barnett, et al., Specific-ion effects on the aggregation mechanisms and protein–protein interactions for anti-streptavidin immunoglobulin gamma-1, J. Phys. Chem. B 119 (18) (May 2015) 5793–5804, https://doi.org/10.1021/acs.jpcb.5b01881.

[14] Q. Luo, Z. Dong, C. Hou, J. Liu, Protein-based supramolecular polymers: progress and prospect, Chem. Commun. 50 (70) (2014) 9997–10007, Aug, https://doi.org/10.1039/C4CC03143A.

[15] M.G. Iadanza, et al., The structure of a β2-microglobulin fibril suggests a molecular basis for its amyloid polymorphism, Nat. Commun. 9 (1) (2018), https://doi.org/10.1038/s41467-018-06761-6. Art. no. 1, Oct.

[16] K. Irie, et al., Structure of β-amyloid fibrils and its relevance to their neurotoxicity: implications for the pathogenesis of Alzheimer's disease, J. Biosci. Bioeng. 99 (5) (May 2005) 437–447, https://doi.org/10.1263/jbb.99.437.

[17] S.M. Kelly, T.J. Jess, N.C. Price, How to study proteins by circular dichroism, Biochimica et Biophysica Acta (BBA) - Proteins and Proteomics 1751 (2) (Aug. 2005) 119–139, https://doi.org/10.1016/j.bbapap.2005.06.005.

[18] A. Barth, C. Zscherp, What vibrations tell us about proteins, Q. Rev. Biophys. 35 (4) (2002) 369–430, https://doi.org/10.1017/s0033583502003815. Nov.

[19] M.F. Pignataro, M.G. Herrera, V.I. Dodero, Evaluation of peptide/protein self-assembly and aggregation by spectroscopic methods, Molecules 25 (Jan. 2020) 20, https://doi.org/10.3390/molecules25204854. Art. no. 20.

[20] Y. Wang, X. Cao, Y. Feng, S. Xue, Environment-induced conformational and functional changes of l-2-haloacid dehalogenase, J. Biosci. Bioeng. 121 (5) (May 2016) 491–496, https://doi.org/10.1016/j.jbiosc.2015.09.008.

[21] D. Tatsubo, K. Suyama, M. Miyazaki, I. Maeda, T. Nose, Stepwise mechanism of temperature-dependent coacervation of the elastin-like peptide analogue dimer, (C(WPGVG)3)2, Biochemistry 57 (10) (2018) 1582–1590, Mar, https://doi.org/10.1021/acs.biochem.7b01144.

[22] T. Shiratori, et al., Singular value decomposition analysis of the secondary structure features contributing to the circular dichroism spectra of model proteins, Biochemistry and Biophy. Rep. 28 (2021), 101153, https://doi.org/10.1016/j.bbrep.2021.101153. Dec.

[23] N. Tonali, V.I. Dodero, J. Kaffy, L. Hericks, S. Ongeri, N. Sewald, Real-time BODIPY-binding assay to screen inhibitors of the early oligomerization process of aβ1-42 peptide, Chembiochem 21 (8) (2020) 1129–1135, Apr, https://doi.org/10.1002/cbic.201900652.

[24] J. Cruz-Angeles, L.M. Martínez, M. Videa, Application of ATR-FTIR spectroscopy to the study of thermally induced changes in secondary structure of protein molecules in solid state, Biopolymers 103 (10) (2015) 574–584, https://doi.org/10.1002/bip.22664.

[25] S. Vatić, N. Mirković, J.R. Milošević, B. Jovčić, N.Đ. Polović, Trypsin activity and freeze-thaw stability in the presence of ions and non-ionic surfactants, J. Biosci. Bioeng. 131 (3) (Mar. 2021) 234–240, https://doi.org/10.1016/j.jbiosc.2020.10.010.

[26] B. Shivu, S. Seshadri, J. Li, K.A. Oberg, V.N. Uversky, A.L. Fink, Distinct β-sheet structure in protein aggregates determined by ATR–FTIR spectroscopy, Biochemistry 52 (31) (2013) 5176–5183, Aug, https://doi.org/10.1021/bi400625v.

[27] D.P. Erickson, O.K. Ozturk, G. Selling, F. Chen, O.H. Campanella, B.R. Hamaker, Corn zein undergoes conformational changes to higher β-sheet content during its self-assembly in an increasingly hydrophilic solvent, Int. J. Biol. Macromol. 157 (Aug. 2020) 232–239, https://doi.org/10.1016/j.ijbiomac.2020.04.169.

[28] Y. Matsuda, et al., Double mutation of cell wall proteins CspB and PBP1a increases secretion of the antibody Fab fragment from Corynebacterium glutamicum, Microb. Cell Factories 13 (1) (2014) 56, https://doi.org/10.1186/1475-2859-13-56.

[29] K. Shiraki, K. Nishikawa, Y. Goto, Trifluoroethanol-induced stabilization of the α-helical structure of β-lactoglobulin: implication for non-hierarchical protein folding, J. Mol. Biol. 245 (2) (Jan. 1995) 180–194, https://doi.org/10.1006/jmbi.1994.0015.

[30] J. Kong, S. Yu, Fourier transform infrared spectroscopic analysis of protein secondary structures, Acta Biochim. Biophys. Sin. 39 (8) (2007) 549–559, https://doi.org/10.1111/j.1745-7270.2007.00320.x. Aug.

[31] E. Goormaghtigh, V. Raussens, J.-M. Ruysschaert, Attenuated total reflection infrared spectroscopy of proteins and lipids in biological membranes, Biochim. Biophys. Acta Rev. Biomembr. 1422 (2) (Jul. 1999) 105–185, https://doi.org/10.1016/S0304-4157(99)00004-0.

[32] G. Baird, C. Farrell, J. Cheung, A. Semple, J. Blue, P.L. Ahl, FTIR spectroscopy detects intermolecular β-sheet formation above the high temperature Tm for two monoclonal antibodies, Protein J. 39 (4) (2020) 318–327, https://doi.org/10.1007/s10930-020-09907-y.

[33] V.V. Shubin, et al., Thermostability of photosystem I trimers and monomers from the cyanobacterium Thermosynechococcus elongatus, Spectrochim. Acta Mol. Biomol. Spectrosc. 179 (May 2017) 17–22, https://doi.org/10.1016/j.saa.2017.02.010.

[34] U.C. Marx, K. Adermann, P. Bayer, W.-G. Forssmann, P. Rösch, Solution structures of human parathyroid hormone fragments hPTH(1–34) and hPTH(1–39) and bovine parathyroid hormone fragment bPTH(1–37), Biochem. Biophys. Res. Commun. 267 (1) (Jan. 2000) 213–220, https://doi.org/10.1006/bbrc.1999.1958.

[35] V. Sathya Devi, D.R. Coleman, J. Truntzer, Thermal unfolding curves of high concentration bovine IgG measured by FTIR spectroscopy, Protein J. 30 (6) (2011) 395–403, https://doi.org/10.1007/s10930-011-9344-y. Aug.

[36] H. Ramshini, R. Tayebee, A. Bigi, F. Bemporad, C. Cecchi, F. Chiti, Identification of novel 1,3,5-triphenylbenzene derivative compounds as inhibitors of hen lysozyme amyloid fibril formation, Int. J. Mol. Sci. 20 (22) (2019) 5558, https://doi.org/10.3390/ijms20225558. Nov.